ARMY RESEARCH LABORATORY

Magnetic Flux Compression Simulations Using ALEGRA

by Robert L. Doney and Peter Bartkowski

ARL-RP-384 **July 2012**

A reprint from the *Proceedings of the ARL Protection Technologies Workshop*, pp 1–12, Aberdeen Proving Ground, MD, May 2012.

NOTICES

Disclaimers

The findings in this report are not to be construed as an official Department of the Army position unless so designated by other authorized documents.

Citation of manufacturer's or trade names does not constitute an official endorsement or approval of the use thereof.

Destroy this report when it is no longer needed. Do not return it to the originator.

Army Research Laboratory
Aberdeen Proving Ground, MD 21005-5066

ARL-RP-384 **July 2012**

Magnetic Flux Compression Simulations Using ALEGRA

Robert L. Doney and Peter Bartkowski
Weapons and Materials Research Directorate, ARL

A reprint from the *Proceedings of the ARL Protection Technologies Workshop*, pp 1–12, Aberdeen Proving Ground, MD, May 2012.

REPORT DOCUMENTATION PAGE	Form Approved OMB No. 0704-0188

1. REPORT DATE *(DD-MM-YYYY)*	2. REPORT TYPE	3. DATES COVERED (From - To)
July 2012	Reprint	1 February 2011–1 April 2012

4. TITLE AND SUBTITLE
Magnetic Flux Compression Simulations Using ALEGRA

5a. CONTRACT NUMBER

5b. GRANT NUMBER

5c. PROGRAM ELEMENT NUMBER

6. AUTHOR(S)
Robert L. Doney and Peter Bartkowski

5d. PROJECT NUMBER

5e. TASK NUMBER

5f. WORK UNIT NUMBER

7. PERFORMING ORGANIZATION NAME(S) AND ADDRESS(ES)
U.S. Army Research Laboratory
ATTN: RDRL-WMP-D
Aberdeen Proving Ground, MD 21005-5066

8. PERFORMING ORGANIZATION REPORT NUMBER
ARL-RP-384

9. SPONSORING/MONITORING AGENCY NAME(S) AND ADDRESS(ES)

10. SPONSOR/MONITOR'S ACRONYM(S)

11. SPONSOR/MONITOR'S REPORT NUMBER(S)

12. DISTRIBUTION/AVAILABILITY STATEMENT
Approved for public release; distribution is unlimited.

13. SUPPLEMENTARY NOTES
A reprint from the *Proceedings of the ARL Protection Technologies Workshop*, pp 1–12, Aberdeen Proving Ground, MD, May 2012.

14. ABSTRACT
Magnetic flux compression (MFC) generators are pulsed-power devices that take a small electrical current and amplify it by exploiting the conservation of magnetic flux. Essentially, an explosive is used to compress an initial magnetic flux into a smaller volume, increasing the output current. The primary benefits of these devices are (1) the reduction in stored electrical energy and (2) obtaining very large currents or magnetic fields. For example, a capacitor bank of 290 kJ can be replaced by an energy-equivalent MFC using only a small explosive weight and a 17-kJ capacitor bank for the seed current. A weight and volume savings of 75–90% can be achieved.

The goal of this effort is to develop the numerical tools necessary to predict the performance of various designs, in order to reduce the number of experiments required. The hardware is destroyed during each test and is expensive to manufacture, making it difficult to perform parametric studies. This report investigates basic flux compression phenomena and inductance modeling. Additionally, we begin to explore flux compression performance improvements by simulating the effects of changing armature velocity and identifying magnetic energy distribution.

15. SUBJECT TERMS
magnetic flux compression, modeling

16. SECURITY CLASSIFICATION OF:			17. LIMITATION OF ABSTRACT	18. NUMBER OF PAGES	19a. NAME OF RESPONSIBLE PERSON
a. REPORT	b. ABSTRACT	c. THIS PAGE			Robert L. Doney
Unclassified	Unclassified	Unclassified	UU	18	19b. TELEPHONE NUMBER (*Include area code*) 410-278-7309

Magnetic flux compression simulations using ALEGRA

Robert L. Doney
Physical Scientist

Peter Bartkowski
Mechanical Engineer

U.S. Army Research Laboratory, Aberdeen Proving Ground, MD 21005-5066
robert.l.doney4.civ@mail.mil

Introduction

Magnetic flux compression (MFC) generators are pulsed-power devices that take a small electrical current and amplify it by exploiting the conservation of magnetic flux. Essentially, an explosive is used to compress an initial magnetic flux into a smaller volume, increasing the output current. The primary benefits of these devices are (1) the reduction in stored electrical energy and (2) obtaining very large currents or magnetic fields. For example, a capacitor bank of 290 kJ can be replaced by an energy equivalent MFC using only a small explosive weight and a 17 kJ capacitor bank for the seed current. A weight and volume savings of 75–90% can be achieved.

The goal of this effort is to develop the numerical tools necessary to predict the performance of various designs, in order to reduce the number of experiments required. The hardware is destroyed during each test and is expensive to manufacture, making it difficult to perform parametric studies. This manuscript investigates basic flux compression phenomena and inductance modeling. Additionally, we begin to explore flux compression performance improvements by simulating the effects of changing armature velocity and identifying magnetic energy distribution.

Flux Compression Basics

Mathematically, one can see how current is amplified through the following. Conservation of magnetic flux requires that the initial and final values must be equal, $\psi_i=\psi_f$. These can be rewritten in terms of electrical inductance, L, and current, i: $L_i i_i = L_f i_f$, which are subsequently rearranged so that

$$G = \frac{I_f}{I_i} = \left(\frac{L_i}{L_f}\right)^{\alpha}, \tag{1}$$

where G is the current gain and α is the system efficiency. Therefore, large initial and small final inductances will help to maximize the gain. For this reason, helical (outer) conductors are typically used since they provide a very large inductance. This is in contrast to solid (coaxial) conductors which have a much lower inductance.

In Figure 1, we see two concentric, cylindrical conductors with explosive filling the inner region (black) and which are linked at the far end by another conductor (not visible). A potential difference is applied between the two conductors which results in a small "seed" current that begins to diffuse into the conductors. This current density (colored) is visible on the clip plane along with contours of the magnetic field strength, *B*. In the image, the explosive has just initiated and a detonation front is propagating radially outward. Eventually, it will make its way down the cylindrical axis pushing the inner conductor radially outward.

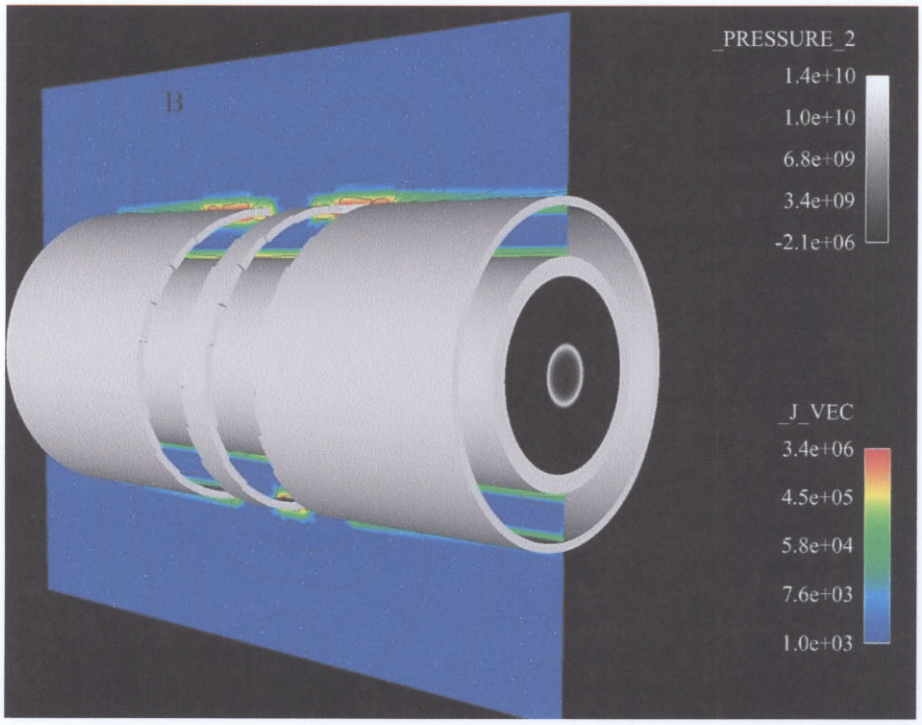

Figure 1. Helical MFC at early time.

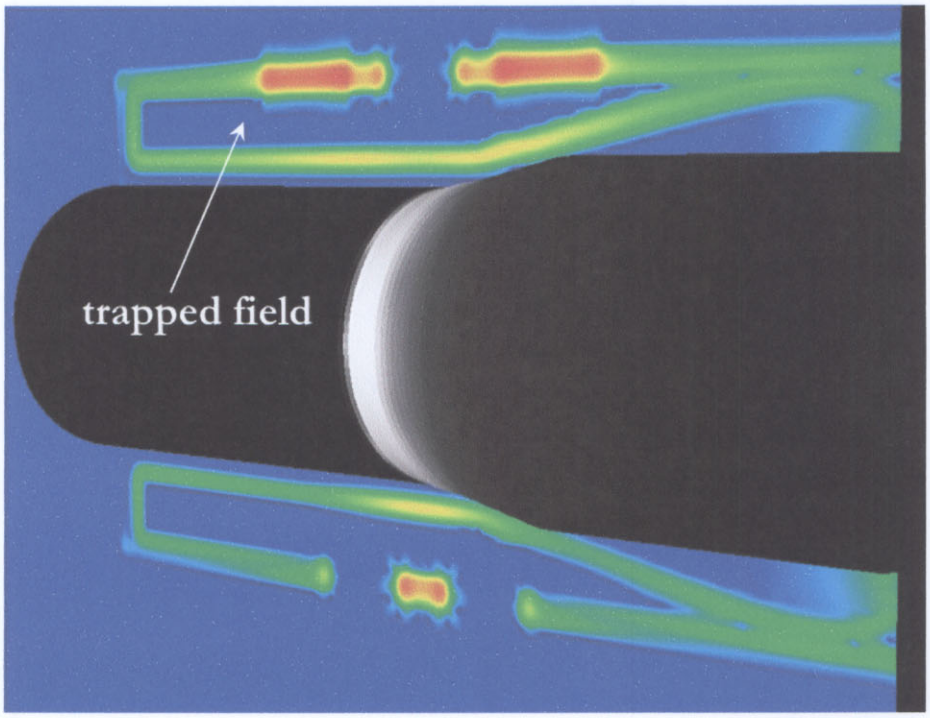

Figure 2. Helical MFC at later time (device not pictured).

Figure 2 illustrates the device at a later time. Here we see the explosive pressure wave has propagated down the MFC and consequently pushed the inner conductor into the outer one—denoted by the (colored) current density. This causes a short circuit such that there is now an increasingly trapped field whose cross-sectional area continues to shrink as the inner conductor is further deformed by the explosive pressure. As this happens, the current density and total current about that region will continue to rise. Also note that, in the final state, no coils are present—similar to a coaxial cable—so that the measured final inductance is very low. Combining that with the large inductance due to coils in the initial state means a high current gain, as equation 1 indicates. For this reason, helical MFCs or "Helicoils" are a favored design geometry for maximizing output current.

In this manuscript we summarize efforts over the past few years of how two-dimensional (2-D) and three-dimensional (3-D) ALEGRA [*1*] simulations have influenced the design of MFC prototypes. A substantial portion of this time was spent ensuring accurate solutions through validation and numerical calibration. Recently, however, the code has been very helpful in understanding phenomenology and encouraging design changes. However, simulating these devices can be challenging for a variety of reasons. As a result, it was necessary to validate individual pieces before moving to greater sophistication: ensuring inductances were correct in both 2-D and 3-D, or that peak currents were converging with appropriate magnetic solver tolerance, for example. It turned out that, while the inductance had converged using a tolerance setting of 10^{-6}, peak current would only converge if the solver setting had a tighter tolerance, 10^{-8}. This was neither obvious or quick to determine. Consequently, this study is broken into several pieces: (1) 2-D and 3-D coaxial cable (no explosive), (2) 3-D Helicoil (no explosive) (3) 2-D

coaxial MFC, and (4) 3-D Helicoil MFC. Each of these efforts will be described, and where appropriate, references to more complete studies will be identified.

2-D and 3-D Coaxial Cable (no explosive)

When no coil is present, the concentric, cylindrical shells have rotational symmetry so the problem can be treated in 2-D. Niederhaus [*2*] has treated this as a verification and validation problem for ALEGRA that will remain in their benchmarks for testing with each new version of the code. To summarize, the inductance for a coaxial cable—excluding any end connection for current return—is given by [*3*],

$$L = \frac{\mu l}{2\pi}\left[-\frac{r_4^4 \ln(r_4/r_3)}{\left(r_4^2 - r_3^2\right)^2} + \frac{\left(3r_4^2 - r_3^2\right)}{4\left(r_4^2 - r_3^2\right)} + \ln\left(\frac{r_2}{r_3}\right) + \frac{r_1^4 \ln(r_1/r_2)}{\left(r_1^2 - r_2^2\right)^2} - \frac{\left(3r_1^2 - r_2^2\right)}{4\left(r_1^2 - r_2^2\right)} \right], \tag{2}$$

where r_4, r_3, r_2, and r_1 represent the inner and outer surfaces of the inner then outer conductors, respectively, and l is the length. Note that, although the geometry is a simple configuration, an exact form for the inductance is quite complicated. For Helicoils, there is no closed-form solution. Niederhaus found that ALEGRA agrees to within 0.1% of theory.

When one adds in a current return, complications arise due to a non-trivial current density in that additional piece. Figure 3 plots inductance converging for both 2-D and 3-D simulations. What one considers to be converged is related to some tolerance of uncertainty. In figure 3, the inductance appears to converge to about 2.645 nH. Bounds are then identified ±0.1% and ±0.5% about this value. Even though we may only be able to use 6–10 cells across the thinnest conductor in a full 3-D simulation, this plot indicates that we would still be within 1% of the converged value. For large Eulerian simulations, that is outstanding agreement.

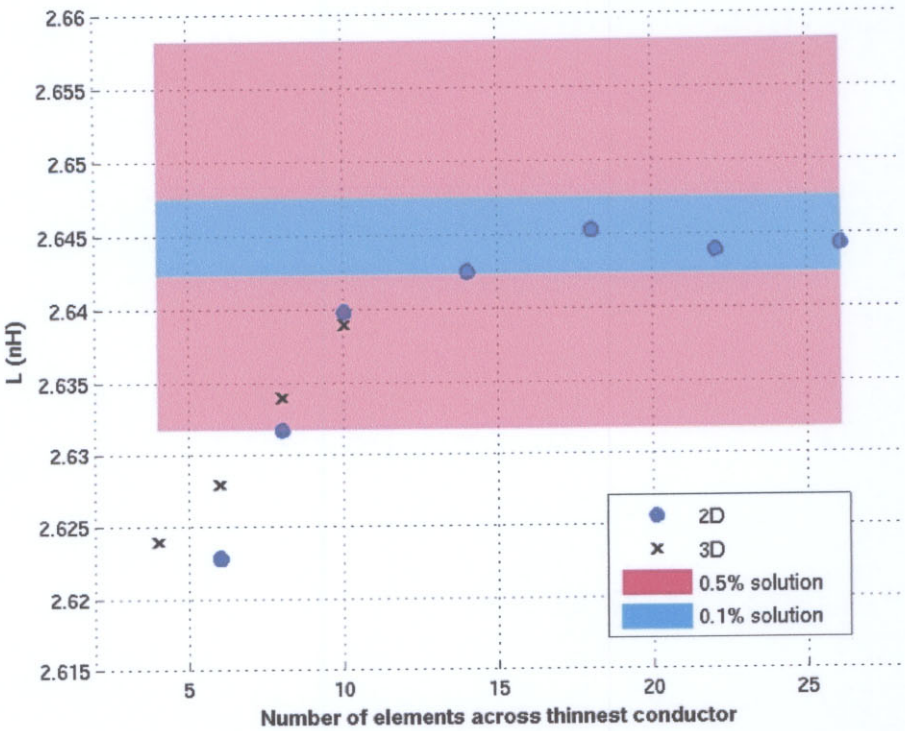

Figure 3. Inductance convergence for a 2-D and 3-D coaxial cable.

3-D Helicoil (no explosive)

With the success of above, we can increase the sophistication by replacing the outer conductor with a coil of rectangular cross-sectional area. We have investigated this problem extensively [*3,4*] and in collaboration with Niederhaus [*5*]. Figure 4 shows typical Helicoils of constant and variable pitch with ten gap twists and nine conducting twists. Pitch is defined as the axial length over which one twist advances. The arrow points out a boundary between the two types of twists. Variable (increasing) pitches are used to prevent the growing current density from melting the device as the inner radial expansion propagates down the axis. The current density is managed by increasing the twists' cross sectional area. When using ten cells across the thinnest conductor, we find that for nine conducting twists, inductance agrees to within about 4% of computationally and experimentally measured values. Further, by selecting a nine-turn, variable-pitch Helicoil, the inductance changes by few percent—agreeing with the expectation that it should be equivalent to the constant pitch case.

By holding the length constant over which the number of twists are allowed to vary, one can obtain details about the steady state inductance, peak current, time to peak current, and inductance at peak current—presuming the requisite convergence analysis has been completed. These are plotted in Figure 5 for one Helicoil design with 1–9 conducting loops. The data indicate that the peak current decreases with increasing twists; however, the time at which peak current occurs increases with the number of twists. This is consistent with the lower left panel which shows that inductance increases with the number of twists (approximately quadratically). Essentially, *di/dt*, or the current rise, is inversely proportional to inductance.

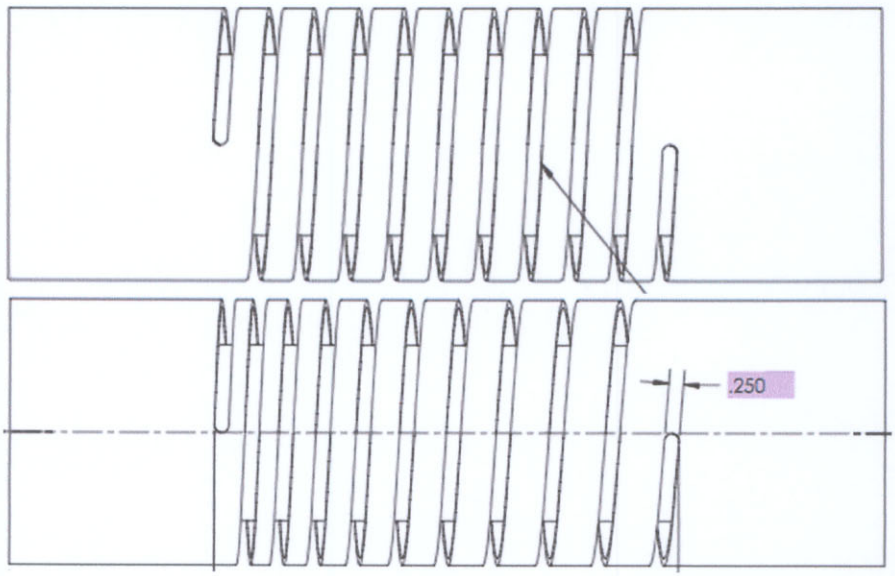

Figure 4. Typical constant and variable pitch Helicoils.

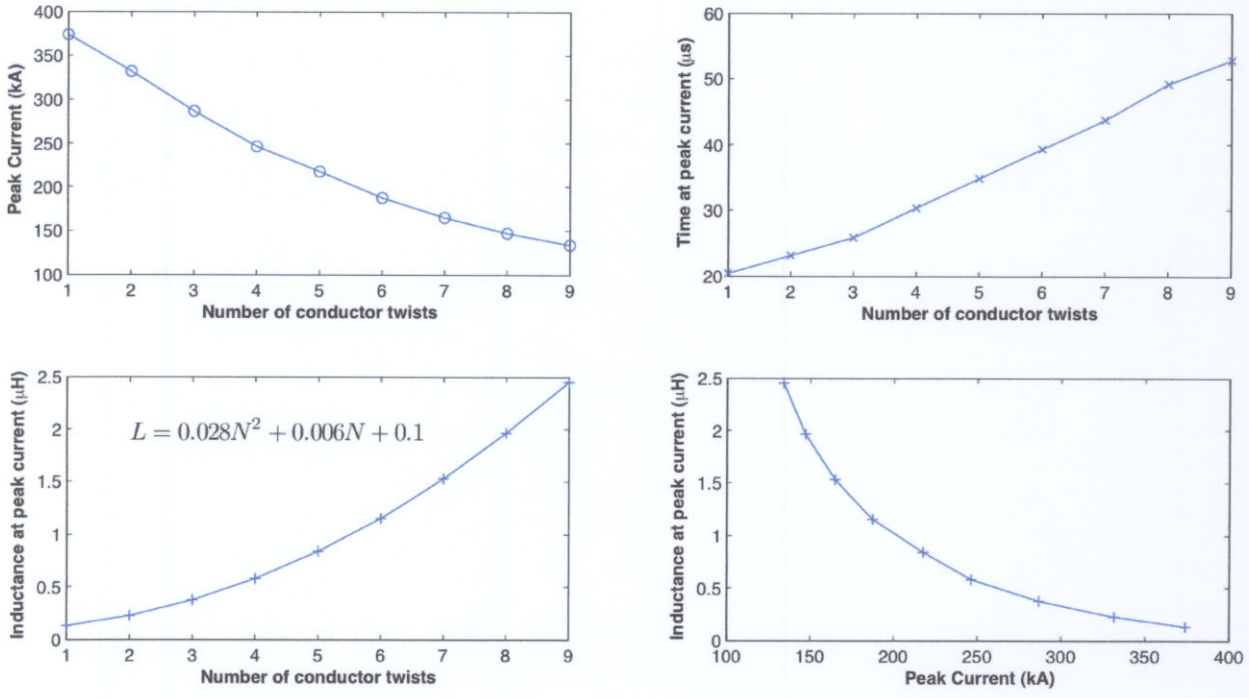

Figure 5. Inductance and current scaling behavior for a Helicoil.

2-D Coaxial MFC

A lot of phenomenology can be investigated with 2-D coaxial MFCs. Two important items we address here are the effects of mesh resolution and armature velocity. Figure 6 illustrates how mesh resolution can affect peak current. Plotted is the amplified current as a function of time for

4, 8, 16, and 24 cells across the thinnest conductor (blue, red, black, and green dashed data series, respectively). At 16 μs, the measured current is still equal to the seed current of 1A. As the upper-left image indicates, flux compression has not started since the inner conductor is still expanding radially outward, but has not impacted the outer conductor. At 27 μs, current amplification has begun since the region of interest is undergoing flux compression. At late times however, the effects of mesh resolution can clearly be seen where approximately *16 cells across the thinnest conductor* are required to converge to within some tight tolerance. This tolerance is probably tighter than it needs to be. However, being converged in one variable (inductance or solver tolerance) does not imply convergence in other relevant variables (e.g. peak current). Indeed, if we were to loosen the solver tolerance here from 10^{-8} to 10^{-6}, peak currents *diverge* with increasing resolution even though the latter is sufficient when measuring inductance only. It should also be pointed out that, up to this point, we have been discussing steady-state inductance where, over a long time, current diffuses throughout the conductor. In many cases, we may want a short diffusion time where the diffusion depth has to be resolved—which can be much thinner than the conductor thickness. Hence, computational cost can increase rapidly even for 2-D simulations.

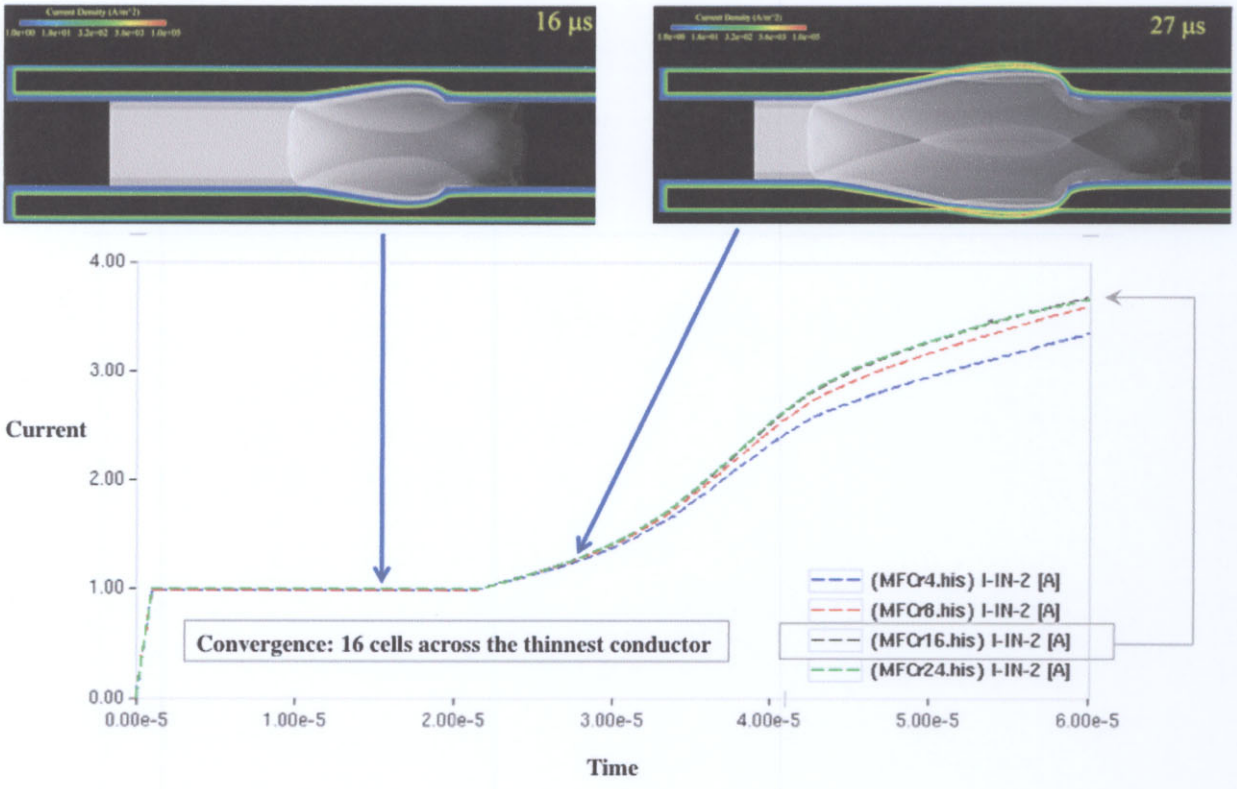

Figure 6. Impact of mesh resolution on current gain for a 2-D coaxial MFC.

Another question we wanted to address with 2-D coaxial MFC was how the armature velocity impacted performance. Rather than a full parametric study, we modeled four specific cases: (1) reference (1/4" phenolic wrap and 1/4" armature), (2) 1/8" phenolic wrap, (3) 1/8" armature, and (4) 1/8" armature and 1/8" phenolic wrap. These configurations are illustrated in Figure 7 and read counter-clockwise starting from the lower right. In these images, the explosive is in yellow

and is encased in a phenolic wrap (green). Conductors are in red, where the armature is in contact with the phenolic wrap. Attached to the outer conductor near the point of detonation is a thin crowbar which allows the flux compression to start earlier. In general, the thicker armatures have more inertia so it is expected that performance will increase with thinner materials or more explosive.

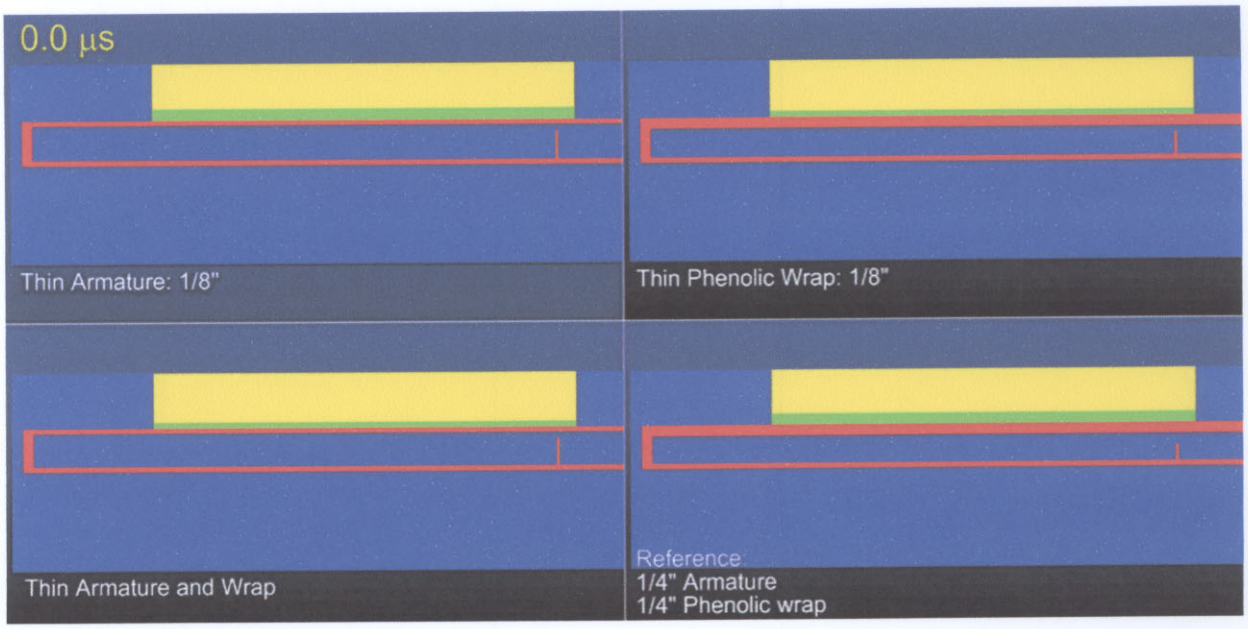

Figure 7. Configurations for evaluating the effects of armature velocity on system performance.

Figure 8 reports the amplified current as a function of time for the four configurations in Figure 7. As expected, the reference configuration displays the poorest performance. The cases of a thin armature and thin high-explosive (HE) wrap show equivalent performance out to about 40 μs when the explosive stops doing work on the radial expansion of the armature. At that point, case 3 provides better flux compression as the thinner metal has a higher radial velocity. In case 4, the analysis is the same: the thinner phenolic wrap is only useful until the explosive stops doing work, the dominant effect then becomes the thickness of the armature. Being equivalent to case 3, performance converges to similar values by 55 μs. In general, case 4—and, arguably case 3—yields a 20% improvement in current gain over the reference case.

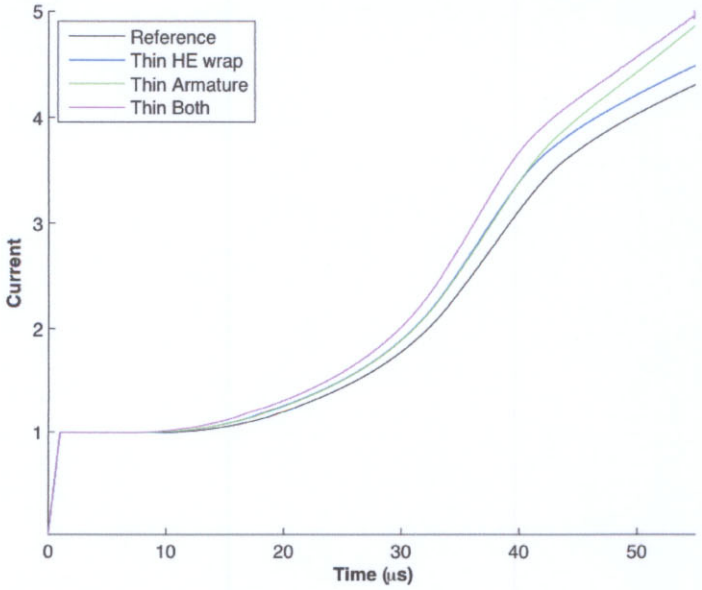

Figure 8. System performance as a function of armature velocity.

3-D Helicoil MFC

Due to the computational cost of 3-D simulations, our Helicoil design is reduced in total length and uses three conducting twists with variable pitch. Some questions we have investigated are (1) what is the magnetic energy distribution and (2) what effect does changing coil material have on current gain?

Quantifying the magnetic energy distribution is another approach for improving performance since magnetic field extends to places where it is simply wasted or leaked which reduces system efficiency. For example, the coils are necessary to maximize the initial inductance; however, they also allow the field to leak out which cannot be used in the flux compression process under current designs. Another measureable loss is field diffusion into the conductors. One example for improving performance might be to increase the magnetic diffusion time so that field only resides on the conductor's surface. This could be accomplished by picking a material with higher electrical conductivity since the magnetic diffusion time, τ, is proportional to conductivity, σ, and a length scale (or thickness), L, over which diffusion occurs: $\tau \sim \sigma L^2$. However, if the EOS is the dominant factor (at critical times) in system performance, changing the conductivity may not be very effective as long as one uses some minimum value typical for metals.

Figure 9 illustrates our approach for quantifying the partition of magnetic energy. In the right-hand side of the image we see the MFC surrogate as well as the magnetic field on a clip plane. The strength of field shown varies over 2 orders of magnitude, and leakage is clearly visible. The magnetic flux through the plane is plotted against time in the upper left for two datasets. The first is the total flux passing through the plane (green line), while the second is just the flux outside of the device (essentially any field crossing the black clip plane). This quantity is obviously smaller (red line). These types of measurements can be difficult to make since the objects being integrated over can deform in time and the visualization software does not always have the requisite tools. We can measure the magnetic energy, E_{Mag}, for several quantities: (1) total

energy, (2) energy inside the conductors, and (3) energy inside the explosive. The lower-left plot shows total magnetic energy (yellow, green dots) and energy in the conductors (purple). To help validate the method in our visualization tool, Ensight, we compared the value computed by ALEGRA (yellow line) with integration over the volume for regions defined by the user, such as conductors or, in this case, the whole computational domain. Both approaches yield the same answer.

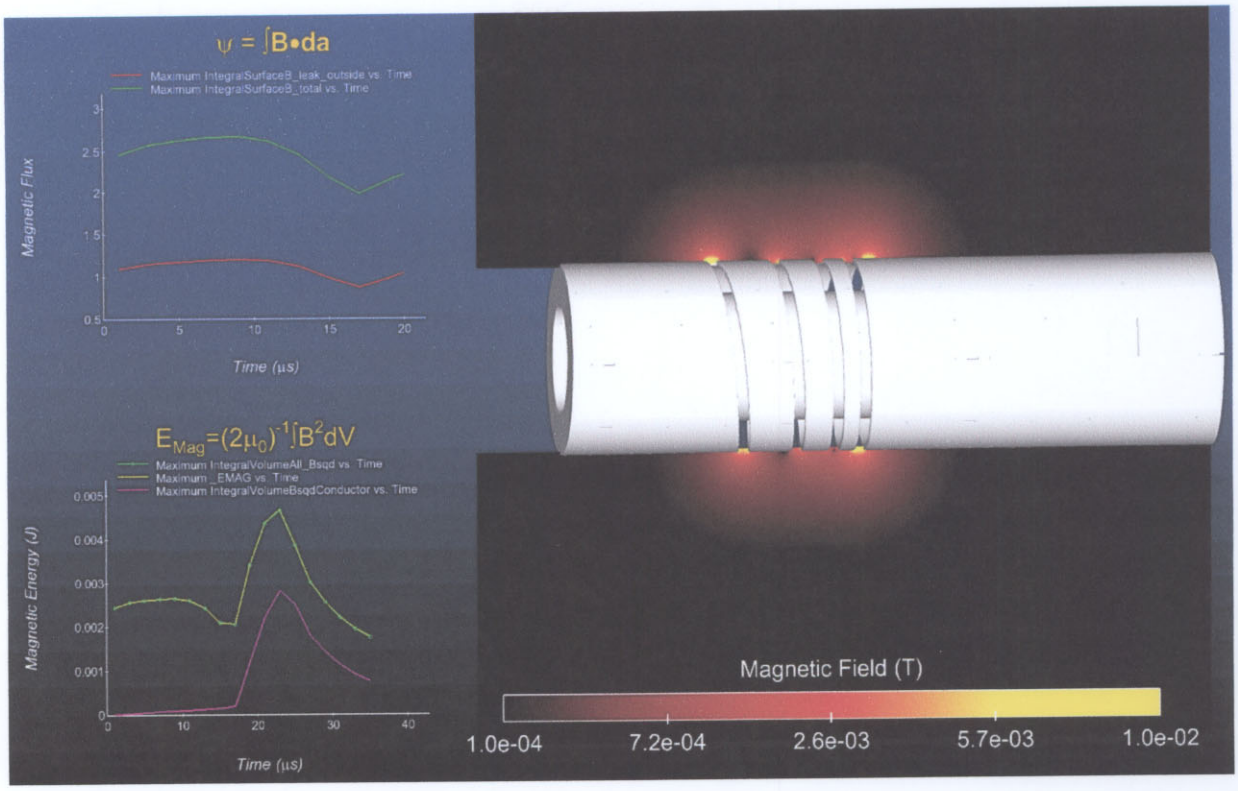

Figure 9. Quantifying magnetic energy partitioning.

We can iterate further and add in magnetic energy stored in the explosive. This data is plotted in Figure 10. As one might expect, the majority of field is initially in air. As current continues to diffuse into the conductors, it's share will rise and it does so up until about 17 μs when the inner conductor has impacted the outer conductor. It's unclear why the explosive value is so high given that, at early time, current hasn't diffused far into the conductor and so the armature should be "shielding" the explosive. This needs to be investigated further. The next step for this type of analysis is to create different pockets of air, so that we can resolve magnetic energy partition inside the compression area and outside the device.

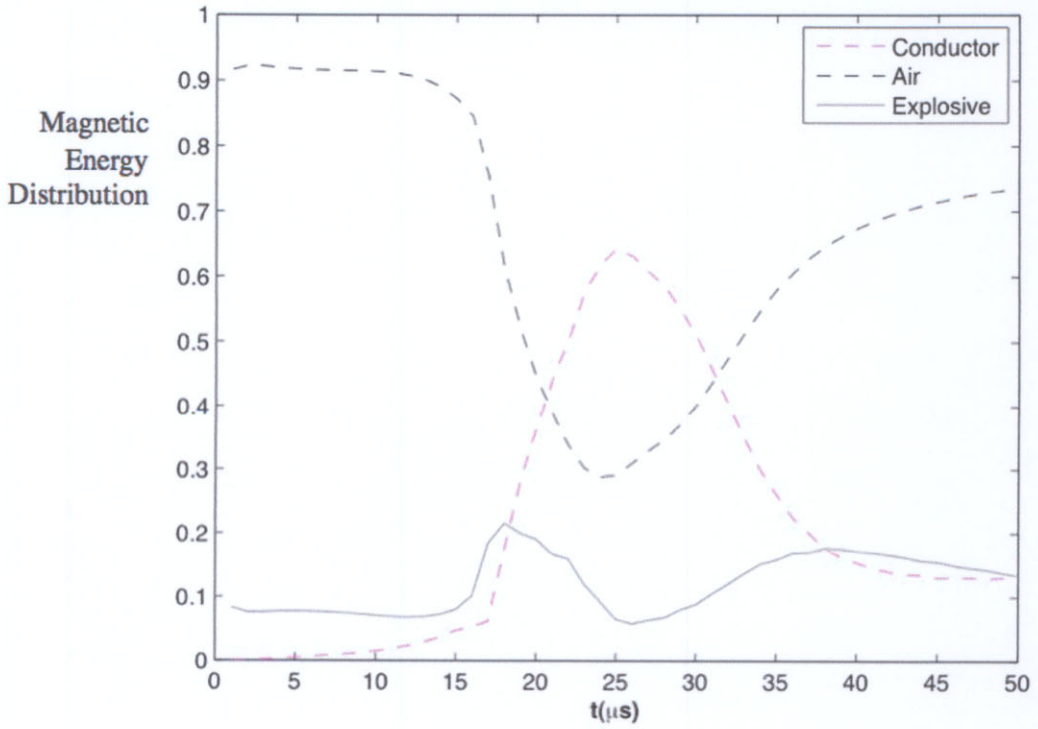

Figure 10. Normalized magnetic energy partitioning.

Conclusion

In this report, we have documented our progress in modeling MFC to improve a design for pulsed power applications. Simulations focused on 2-D and 3-D coaxial and helical MFCs with and without explosive. These results have provided a link between increased system performance and armature velocity. Further, ALEGRA simulations are quantifying the partitioning of magnetic energy which will guide us in minimizing leakage and other losses.

References

[1] Robinson, A., *et al.* "Alegra user manual," Sandia National Laboratories, November 2011.
[2] Niederhaus, J.H., "Verification for simulating magnetic diffusion in a simple coaxial cable." Sandia National Laboratories Technical Report, *to be submitted.*
[3] Doney, R.L., "Inductance scaling of a Helicoil using ALEGRA." U.S. Army Research Laboratory Technical Report, *to be submitted.*
[4] Bartkowski, P., and Berning, P. "Inductance calculations of variable pitch helical inductors." U.S. Army Research Laboratory Technical Report, *in press.*
[5] Niederhaus, J.H., Personal communications, 2011.

NO. OF COPIES	ORGANIZATION
1 (PDF only)	DEFENSE TECHNICAL INFORMATION CTR DTIC OCA 8725 JOHN J KINGMAN RD STE 0944 FORT BELVOIR VA 22060-6218
1	DIRECTOR US ARMY RESEARCH LAB IMNE ALC HRR 2800 POWDER MILL RD ADELPHI MD 20783-1197
1	DIRECTOR US ARMY RESEARCH LAB RDRL CIO LL 2800 POWDER MILL RD ADELPHI MD 20783-1197

NO. OF
COPIES ORGANIZATION

2 SANDIA NATIONAL LABORATORIES
E STRACK MS 1323
J NIEDERHAUS MS 1323
BOX 5800
ALBUQUERQUE NM 87185-1323

1 SANDIA NATIONAL LABORATORIES
C SIEFERT MS 1322
BOX 5800
ALBUQUERQUE NM 87185-1322

1 SANDIA NATIONAL LABORATORIES
K COCHRANE MS 1189
BOX 5800
ALBUQUERQUE NM 87185-1189

1 SANDIA NATIONAL LABORATORIES
C GARASI MS 0380
BOX 5800
ALBUQUERQUE NM 87185-0380

ABERDEEN PROVING GROUND

21 DIR USARL
RDRL WMP A
P BERNING
C HUMMER
A PORWITZKY
C UHLIG
J POWELL
RDRL WMP B
J MCDONALD
S SATAPATHY
RDRL WMP C
J HOUSKAMP
RDRL WMP D
A BARD
R DONEY (3 CPS)
M KEELE
F MURPHY
G VUNNI
RDRL WMP E
S BARTUS
P BARTKOWSKI
B CHAMISH
D HACKBARTH
D HORNBAKER
C KRAUTHAUSER

INTENTIONALLY LEFT BLANK.